

## Article

# Slow Magnetic Relaxation in a [Co<sub>4</sub>O<sub>4</sub>] Cubane Complex with Tridentate NNO-Schiff Base Ligands

Yuki Suemitsu<sup>1</sup>, Yoshitaka Amakusa<sup>1</sup>, Haruka Yoshino<sup>2</sup>, Masaaki Ohba<sup>3</sup> and Masayuki Koikawa<sup>1,\*</sup> 

<sup>1</sup> Department of Chemistry and Applied Chemistry, Faculty of Science and Engineering, Saga University, Honjo 1, Saga 840-8502, Japan; suemitsu@koi-ken.info (Y.S.)

<sup>2</sup> Institute for Materials Research, Tohoku University, 2-1-1 Katahira, Aoba-ku, Sendai 980-8577, Japan; haruka.yoshino.a2@tohoku.ac.jp

<sup>3</sup> Department of Chemistry, Faculty of Science, Kyushu University, 744 Motooka, Nishi-ku, Fukuoka 819-0395, Japan; ohba@chem.kyushu-univ.jp

\* Correspondence: koikawa@cc.saga-u.ac.jp

**Abstract:** Two tetranuclear Co(II) complexes, [Co<sub>4</sub>(pmab)<sub>4</sub>Cl<sub>4</sub>] (1) and [Co<sub>4</sub>(pmab)<sub>4</sub>(OBz)<sub>2</sub>]Cl<sub>2</sub> (2) [Hpmab = 2-((*p*-pyridinylmethylene)amino)benzenemethanol], have been synthesized and characterized through single-crystal X-ray diffraction, IR and UV-VIS spectroscopy, and magnetic measurements. Structural analysis revealed that both complexes possess a [Co<sub>4</sub>O<sub>4</sub>] cubane-like metal core connected by μ<sub>3</sub>-alkoxo bridges. Magnetic measurements of Complex 1 indicate weak ferromagnetic interactions ( $J \sim +0.75 \text{ cm}^{-1}$ ) within the tetranuclear core, while Complex 2 exhibits antiferromagnetic behavior due to the presence of *syn-syn* bridging benzoate ligands. Alternating current (AC) magnetic measurements suggest that Complex 1 exhibits slow magnetic relaxation behavior.

**Keywords:** tetranuclear complex; cobalt; crystal structure; cubane; Schiff base ligand; magnetic property



**Citation:** Suemitsu, Y.; Amakusa, Y.; Yoshino, H.; Ohba, M.; Koikawa, M. Slow Magnetic Relaxation in a [Co<sub>4</sub>O<sub>4</sub>] Cubane Complex with Tridentate NNO-Schiff Base Ligands. *Magnetochemistry* **2024**, *10*, 85. <https://doi.org/10.3390/magnetochemistry10110085>

Academic Editor: Marius Andruh

Received: 30 September 2024

Revised: 29 October 2024

Accepted: 29 October 2024

Published: 30 October 2024



**Copyright:** © 2024 by the authors. Licensee MDPI, Basel, Switzerland. This article is an open access article distributed under the terms and conditions of the Creative Commons Attribution (CC BY) license (<https://creativecommons.org/licenses/by/4.0/>).

## 1. Introduction

Since the discovery of the single-molecule magnet (SMM) properties of the Mn<sub>12</sub> cluster in 1993 [1], numerous magnetic molecules exhibiting slow magnetic relaxation have been synthesized and extensively studied over the past 30 years [2–6]. These SMMs, with their high relaxation barriers ( $U_{\text{eff}}$ ) and blocking temperatures ( $T_{\text{B}}$ ), hold promise for applications in quantum computing, spintronic devices, and high-density data storage [7,8]. This potential has driven the development of SMMs with enhanced performance [9–11].

Two key factors that determine the  $U_{\text{eff}}$  and  $T_{\text{B}}$  of SMMs are a large ground-state spin ( $S$ ) and a large negative zero-field splitting parameter ( $D$ ). While early SMM research focused on Mn(III) and Fe(III) [12,13], cobalt-based SMMs remained relatively unexplored due to their typically large positive  $D$  values. However, it has been suggested that in cubane structures, a negative  $D$  value can be achieved by designing the cubane motif to promote dominant ferromagnetic interactions within the tetranuclear metal core and optimize the orthogonality of the anisotropy axes of individual metal ions [14]. Based on this premise, the tetranuclear Co(II) complex [Co<sub>4</sub>(hmp)<sub>4</sub>(MeOH)<sub>4</sub>Cl<sub>4</sub>] (Hhmp = 2-hydroxymethylpyridine) was synthesized, exhibiting magnetic hysteresis due to the ground-state spin of  $S_{\text{T}} = 6$  and negative magnetic anisotropy ( $D_{\text{mol}} < 0$ ) [15]. Moreover, examples of Co(II) single-ion magnets (SIMs) exhibiting slow magnetic relaxation even when  $D_{\text{ion}} > 0$  have been reported [16,17]. Since these discoveries, research on Co(II)-based SMMs and SIMs has progressed rapidly, and in particular, polynuclear clusters with the [Co<sub>4</sub>O<sub>4</sub>] cubane core as a structural motif have been reported [18–21]. In recent study, a [Co<sub>7</sub>O<sub>12</sub>] cluster [22] and a [Co<sub>4</sub>O<sub>4</sub>]<sub>3</sub> cluster [23], both featuring extended cubane structure, have garnered attention not only in the field of magnetochemistry but also as nanomaterials.

The cubane-type [M<sub>4</sub>O<sub>4</sub>] motif has been widely reported as a structural feature in the magnetochemistry of first-row transition metals, appearing in many complexes including [Mn<sub>4</sub>O<sub>4</sub>], [Ni<sub>4</sub>O<sub>4</sub>], and [Cu<sub>4</sub>O<sub>4</sub>] [24–26]. These complexes are often synthesized

using chelating ligands with hydroxyl groups, which facilitate the formation of cubane-like structures due to their high bridging and chelating abilities. *NO*-type bidentate ligands, such as Hhmp used in  $[\text{Co}_4(\text{hmp})_4(\text{MeOH})_4\text{Cl}_4]$ , are commonly employed due to their ease of synthesis and availability from commercial sources. However, these bidentate ligands cannot fully occupy the coordination sites of the cubane core, leading to the coordination of solvent molecules. These solvent molecules can dissociate from the metal ions under varying temperature or pressure conditions, potentially destabilizing the molecular structure. To address this issue and improve the stability of these complexes for practical applications as magnetic materials, it is essential to design complexes using tridentate or tetradentate chelating ligands rather than simple bidentate ligands [27,28]. These ligands can effectively occupy the coordination sites of the cubane core, preventing solvent coordination and enhancing the structural stability of the complexes.

In our study, we focused on synthesizing polynuclear complexes using tridentate ligands featuring an *o*-aminobenzyl alcohol structure [29,30]. In this research, we successfully synthesized two new tetranuclear Co(II) complexes with a  $[\text{Co}_4\text{O}_4]$  cubane core,  $[\text{Co}_4(\text{pmab})_4\text{Cl}_4]$  (**1**) and  $[\text{Co}_4(\text{pmab})_4(\text{OBz})_2]\text{Cl}_2$  (**2**), using the *NNO*-type tridentate ligand Hpmb [2-((2-pyridinylmethylene)amino)benzenemethanol] (Figure 1). These complexes are unique in that they lack removable coordinating solvent molecules in their cubane cores, significantly reducing the risk of ligand dissociation and subsequent complex decomposition. This enhanced stability is crucial for the practical application of these complexes as magnetic materials. This paper reports the synthesis, molecular structures, and magnetic properties of these tetranuclear Co(II) complexes, as well as the slow magnetic relaxation phenomenon observed in Complex 1.

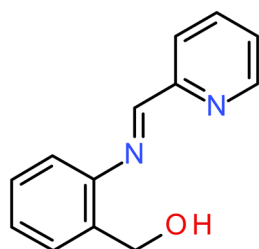


Figure 1. Chemical diagram of Hpmb.

## 2. Materials and Methods

### 2.1. Preparation

All chemicals were used as received unless otherwise noted. Methanol was purified by distillation over magnesium turnings.

#### 2.1.1. Hpmb

To a methanol solution (20 mL) of 2-aminobenzyl alcohol (2.432 g, 20 mmol), 2-pyridinecarboxaldehyde (2.142 g, 20 mmol) was added dropwise with stirring. The resulting mixture was refluxed for 4 h, then filtered and allowed to stand at room temperature. The resulting yellowish-orange solution was concentrated in vacuo to remove all solvent. The crude ligand, obtained as an oily substance, was used in the complexation reactions without further purification. IR (ATR)  $[\text{cm}^{-1}]$ : 3331 (w), 2842 (w), 1609 (m), 1590 (m), 1494 (s), 1470 (vs), 1424 (s), 1365 (m), 1303 (m), 1253 (m), 1048 (s), 748 (vs), 623 (m).

#### 2.1.2. $[\text{Co}_4(\text{pmab})_4\text{Cl}_4]$ (**1**)

To a methanol solution (10 mL) containing cobalt(II) chloride hexahydrate (0.119 g, 0.5 mmol) and Hpmb (0.106 g, 0.5 mmol), a methanol solution (2 mL) of potassium *t*-butoxide (0.011 g, 0.1 mmol) was slowly added over 30 min. The solution turned dark orange, and after 20 min, orange microcrystals suitable for X-ray analysis were obtained.  $1.5\text{H}_2\text{O}$ ; Yield: 0.078 g, 48%.  $\text{C}_{52}\text{H}_{54}\text{Cl}_4\text{Co}_4\text{N}_8\text{O}_9$ : C, 47.58; H, 4.15; N, 8.54%. Found: C, 47.51; H, 3.77; N, 8.50%. IR (ATR)  $[\text{cm}^{-1}]$ : 2873 (vw), 1597 (s), 1493 (m), 1442 (m), 1366 (m),

1241 (m), 1190 (m), 1156 (m), 1018 (vs), 776 (vs), 746 (s), 720 (m), 624 (s). UV-VIS (reflectance) [ $10^3 \text{ cm}^{-1}$ ]: 8.7, 14.4, 14.9, 15.8.

### 2.1.3. $[\text{Co}_4(\text{pmab})_4(\text{OBz})_2]\text{Cl}_2$ (**2**)

A methanol solution (10 mL) containing cobalt(II) chloride hexahydrate (0.119 g, 0.5 mmol) and Hpmb (0.106 g, 0.5 mmol) was prepared. Sodium benzoate (0.072 g, 0.5 mmol) was then added to the solution, resulting in a dark orange color. The solution was slowly concentrated at room temperature over one day, yielding orange single crystals suitable for X-ray analysis.  $2 \cdot 2\text{CH}_3\text{OH}$ ; Yield: 0.018 g, 9.9%.  $\text{C}_{66}\text{H}_{54}\text{Cl}_2\text{Co}_4\text{N}_8\text{O}_8$ : C, 56.02; H, 4.29; N, 7.69%. Found: C, 55.90; H, 3.95; N, 7.43%. IR (ATR) [ $\text{cm}^{-1}$ ]: 2856 (w), 1593 (s), 1551 (vs), 1492 (w), 1399 (vs), 1371 (s), 1304 (m), 1190 (m), 1017 (s), 773 (s), 723 (vs), 679 (m), 623 (m). UV-VIS (reflectance) [ $10^3 \text{ cm}^{-1}$ ]: 8.9, 14.2, 15.0, 15.9.

## 2.2. Measurements

Elemental analyses for C, H, and N were obtained at the Elemental Analysis Service Center, Kyushu University. Infrared spectra were recorded on a Bruker VERTEX70-S FT-IR Spectrometer (Bruker Corp., Billerica, MA, USA) using the attenuated total reflection (ATR) method. UV-VIS reflection spectra were obtained using a PERKIN ELMER Lambda900Z UV/VIS/NIR Spectrometer (PerkinElmer Inc., Waltham, MA, USA) and an Ocean Optics USB2000+ Fiber Optic Spectrometer (Ocean Optics Inc., Dunedin, FL, USA). Magnetic susceptibilities were measured using a Quantum Design MPMS-XL5R SQUID (Superconducting Quantum Interference Device) susceptometer (Quantum Design Inc., San Diego, CA, USA) under an applied magnetic field of 0.1 T in the temperature range 2–300 K. The susceptibilities were corrected for the diamagnetism of the constituent atoms using Pascal's constant [31].

## 2.3. Single Crystal X-Ray Diffraction

Diffraction data were collected on a Rigaku Vari-Max Saturn CCD 724 diffractometer (Rigaku Corp, Tokyo, Japan) with graphite-monochromated Mo K $\alpha$  radiation ( $\lambda = 0.71069 \text{ \AA}$ ) at the Analytical Research Center for Experimental Sciences, Saga University. Data collection was performed using CrystalClear SM 2.0 r16 [32]. The crystal was kept at 113 K during data collection, and multi-scan correction for absorption was applied. Data processing was performed using CrysAlisPro 42.49 [33] for **1** and CrystalClear for **2**. The crystal data and experimental parameters are summarized in Table S1. Structures were solved by direct methods (ShelXT-2016/6) and expanded using Fourier techniques [34]. Non-hydrogen atoms were refined anisotropically, while hydrogen atoms were placed geometrically in calculated positions and refined with a riding model. For Complex **2**, BASF/TWIN refinement was applied. Solvent masks were calculated for disordered solvent molecules [35]. For Complex **1**, 360 electrons were found in a volume of  $1360 \text{ \AA}^3$  in one void per unit cell, and 854 electrons were found in a volume of  $3271 \text{ \AA}^3$  in one void per unit cell for **2**. These are consistent with the presence of  $8[\text{H}_2\text{O}]$  and  $12[\text{CH}_3\text{OH}]$  per molecular formula for **1** and **2**, respectively. The final cycle of full-matrix least-squares refinement on  $F^2$  using ShelXL-2016/6 [36] was based on observed reflections and variable parameters and converged with unweighted and weighted agreement factors of  $R$  and  $R_w$ . Olex2-1.5 [37] was used as an interface to the ShelX program package. The molecular structures were drawn using Mercury-2022.1.0 [38].

## 3. Results and Discussion

### 3.1. Synthetic Outcomes and Characterization

The tridentate ligand Hpmb was isolated as a crude product, and its formation was confirmed by FT-IR spectroscopy (Figure S1). The disappearance of the C=O stretching peak at  $1710 \text{ cm}^{-1}$ , characteristic of 2-pyridinecarboxaldehyde, and the appearance of the C=N stretching vibration at  $1609 \text{ cm}^{-1}$ , indicated the formation of a Schiff base. Additionally, the C–O stretching vibration at  $1048 \text{ cm}^{-1}$ , attributed to the benzyl alcohol moiety,

was observed. In the FT-IR spectrum of **1** (Figure S2), the strong and characteristic bands corresponding to the azomethine  $\nu(\text{C}=\text{N})$  and alcoholic  $\nu(\text{C}-\text{O})$  stretching vibrations of the ligand were shifted to lower frequencies, appearing at  $1597$  and  $1018\text{ cm}^{-1}$ , respectively [22]. This significant shift in the  $\nu(\text{C}-\text{O})$  band suggests the formation of a  $\mu$ -alkoxo bridged structure [27]. For Complex **2**, similar IR bands were observed at  $1593$  and  $1017\text{ cm}^{-1}$  (Figure S3). Additionally, the asymmetric and symmetric carboxylate stretching bands,  $\nu_{\text{as}}(\text{COO})$  and  $\nu_{\text{s}}(\text{COO})$ , were observed at  $1551$  and  $1399\text{ cm}^{-1}$ , respectively. The separation value ( $\Delta$ ) between the  $\nu_{\text{as}}(\text{COO})$  and  $\nu_{\text{s}}(\text{COO})$  frequencies was  $152\text{ cm}^{-1}$ , indicating that the benzoate ion coordinates to the Co(II) ions in a *syn-syn* bridging mode [39]. Elemental analysis results for **1** and **2** showed good agreements between the found and calculated values for the composition of  $[\text{Co}_4\text{Cl}_4(\text{pmab})_4(\text{H}_2\text{O})_5]$  and  $[\text{Co}_4\text{Cl}_2(\text{OBz})_2(\text{pmab})_4(\text{CH}_3\text{OH})_2]$ , respectively.

### 3.2. Structural Studies

The molecular structure of **1** is illustrated in Figure 2a, and selected bond distances and angles are summarized in Table 1. Complex **1** crystallizes in the tetragonal space group  $I4_1/a$ , where the asymmetric unit contains one  $[\text{Co}(\text{pmab})\text{Cl}]$  unit. The tridentate ligand coordinated to Co(II) ion in a meridional mode. The metal core of this tetranuclear complex consists of four Co(II) ions and four  $\mu_3$ -bridging oxygen atoms from the deprotonated  $(\text{pmab})^-$  ligands, forming a  $[\text{Co}_4\text{O}_4]$  cubane structure. Each Co(II) ion adopts an octahedral geometry, with its six coordination sites occupied by three  $\mu_3$ -oxygen atoms, two nitrogen atoms, and one chloride ion. The Co–O and Co–N bond lengths range from  $2.028(3)$  to  $2.194(3)\text{ \AA}$  and  $2.103(3)$  to  $2.169(3)\text{ \AA}$ , respectively. In contrast, the Co1–Cl1 bond length of  $2.4762(12)\text{ \AA}$ . Notable differences exist in the lengths of the three principal axes in the octahedral geometry around Co1. Specifically, the distances between coordinated atoms along these axes are  $4.083(4)\text{ \AA}$  for O1–Co1–N2,  $4.255(4)\text{ \AA}$  for O1'–Co1–N1 [symmetry code: (')  $1 - x, 3/2 - y, +z$ ], and  $4.653(3)\text{ \AA}$  for O1''–Co1–Cl1 [symmetry code: ('')  $5/4 - y, 1/4 + x, 5/4 - z$ ], suggesting a pronounced rhombic distortion in the octahedral environment of Co1. SHAPE analysis values for Co1, with OC-6 and TPR-6 indices of 2.817 and 9.101, respectively, further confirm this significant distortion [40].

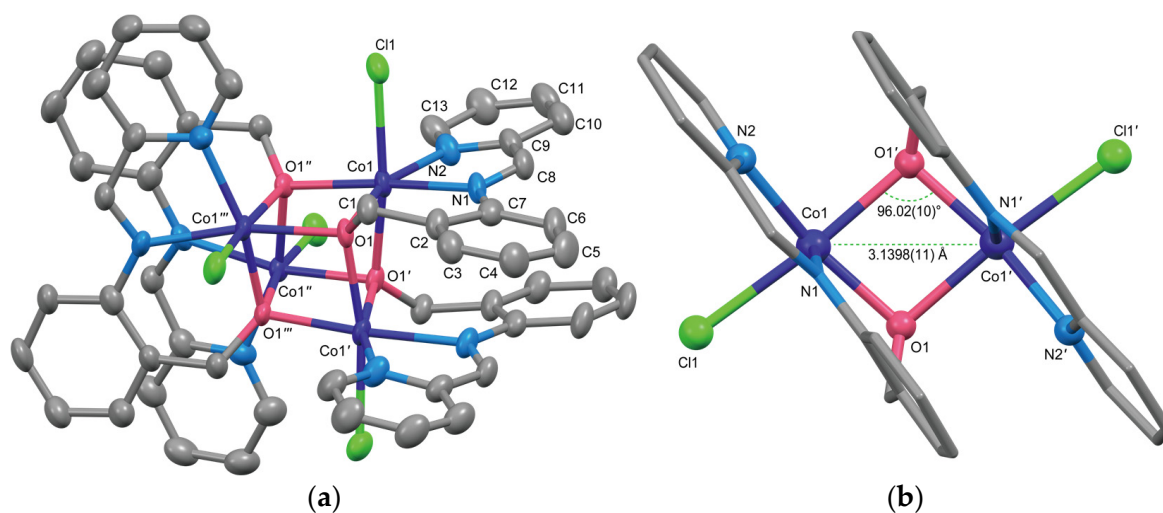


**Figure 2.** (a) Crystal structure for **1**, showing thermal ellipsoids at a 50% probability level. Hydrogen atoms are omitted for clarity. Symmetry Code: (')  $1 - x, 3/2 - y, +z$ ; ('')  $5/4 - y, 1/4 + x, 5/4 - z$ ; ('''')  $-1/4 + y, 5/4 - x, 5/4 - z$ . (b) Structure of the dinuclear unit viewed from the  $\text{Co}_2\text{O}_2$  plane.

**Table 1.** Selected bond distances and angles of **1**.

Bond	Distance/Å	Angle	Angle/°
Co1–Cl1	2.4763(12)	Cl1–Co1–O1′	170.11(7)
Co1–O1	2.028(3)	O1–Co1–N2	162.00(12)
Co1–O1′	2.194(3)	O1′–Co1–N1	168.09(12)
Co1–O1″	2.109(2)	O1–Co1–N1	87.13(11)
Co1–N1	2.169(3)	N1–Co1–N2	77.81(13)
Co1–N2	2.103(3)	O1–Co1–O1″	81.19(10)
Co1⋯Co1′	3.1398(11)	O1″–Co1–N2	114.09(12)
Co1⋯Co1″	3.2371(7)	Co1–O1–Co1′	96.03(10)
		Co1–O1–Co1″	102.96(11)
		Co1′–O1–Co1″	97.56(10)

Symmetry code: (′)  $1 - x, 3/2 - y, +z$ ; (″)  $5/4 - y, 1/4 + x, 5/4 - z$ ; (″″)  $-1/4 + y, 5/4 - x, 5/4 - z$ .

The overall structure can fundamentally be regarded as a dimer-of-dimers configuration, composed of bis- $\mu_2$ -alkoxo-bridged dicobalt units. The structure of the dicobalt unit is depicted in Figure 2b. Generally, in dinuclear structures with planar tridentate ligands, these ligands typically lie within the dinuclear plane. However, in Complex **1**, the chloride ion is positioned within the dinuclear plane, causing the (pmab)<sup>−</sup> ligand to adopt a meridional coordination mode via the axial direction relative to the dinuclear plane. The coordination of the chloride ion within the dinuclear plane also results in variations in the Co–O distances within the Co<sub>2</sub>O<sub>2</sub> unit. The Co–O distance from Co1 to the chelated oxygen O1 is 2.028(3) Å, while the distance to the bridging oxygen O1′ trans to the chloride ion is Co1–O1′ = 2.194(3) Å, approximately 0.17 Å longer. Consequently, the Co<sub>2</sub>O<sub>2</sub> square in the dinuclear unit of **1** takes the shape of a parallelogram. Additionally, the Co1–O1″ distance, which corresponds to the stacking distance between the dinuclear units, is 2.109(2) Å, differing from any of the Co–O distances within the dinuclear plane. The intramolecular metal-to-metal distances are Co1⋯Co1′ = 3.1398(11) Å and Co1⋯Co1″ = 3.2371(7) Å. The bridging angles around the O1 atom are Co1–O1–Co1′ = 96.03(10)°, Co1–O1–Co1″ = 102.96(11)° [symmetry code: (″″)  $-1/4 + y, 5/4 - x, 5/4 - z$ ], and Co1′–O1–Co1″ = 97.56(10)°. Since all these angles are all greater than 90°, the [Co<sub>4</sub>O<sub>4</sub>] cubane core is highly distorted, forming a triakis tetrahedron with four Co vertices.

Each of the four (pmab)<sup>−</sup> ligands in **1** engages in  $\pi$ - $\pi$  stacking with four different neighboring molecules. The two aromatic rings within the tridentate ligand—the phenyl ring of the benzyl alcohol moiety and the pyridine ring—stack with the pyridine and phenyl rings of neighboring molecules, respectively, at a distance of 3.804(3) Å (Figure 3a). As a result, the cubane complexes function as building bricks, forming an ordered 3-D structure, as shown in Figures 3b and S4.

Figure 4a shows the structure of the complex cation of **2**, and selected bond distances and angles are summarized in Table 2. Complex **2** is an ionic compound containing two chloride anions and crystallizes in the tetragonal chiral space group  $I42d$  with  $Z = 4$ . A Flack parameter of 0.48 suggests racemic twinning. The asymmetric unit of **2** contains half of the [Co<sub>2</sub>(pmab)<sub>2</sub>(OBz)]<sup>+</sup>Cl<sup>−</sup> binuclear unit. Similar to **1**, Complex **2** features a [Co<sub>4</sub>O<sub>4</sub>] cubane core and a dimer-of-dimers structure. However, a key difference is the presence of *syn-syn* bridging benzoate ions. The dicobalt structure is illustrated in Figure 4b. Unlike Complex **1**, the ligands in **2** are coplanar with the Co<sub>2</sub>O<sub>2</sub> dinuclear plane, and the benzoate anion binds to the Co atoms axially. The bond distances between the metal ions and coordinating atoms within the dinuclear plane range from 2.127(5) to 2.184(7) Å, while the axial bond distances are slightly shorter, ranging from 2.077(5) to 2.091(5) Å, indicating compressed axial distortion. The SHAPE calculation result (OC-6) of 1.696, smaller than that of **1**, suggests a less distorted geometry overall.

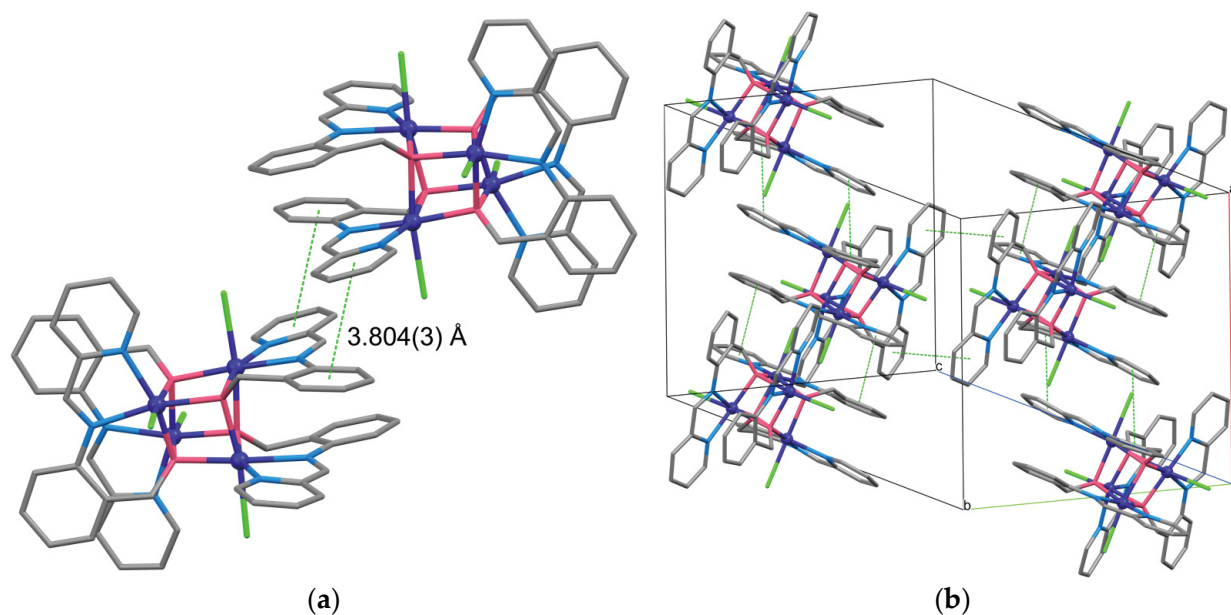


**Figure 3.** (a) Diagram of  $\pi$ - $\pi$  stacking interactions between adjacent complex molecules. Green dotted lines indicate guide lines connecting the centroids of the aromatic rings. Hydrogen atoms are omitted for clarity. (b) Packing diagram with guide lines for  $\pi$ - $\pi$  stacking. Hydrogen atoms and solvent molecules are omitted for clarity.

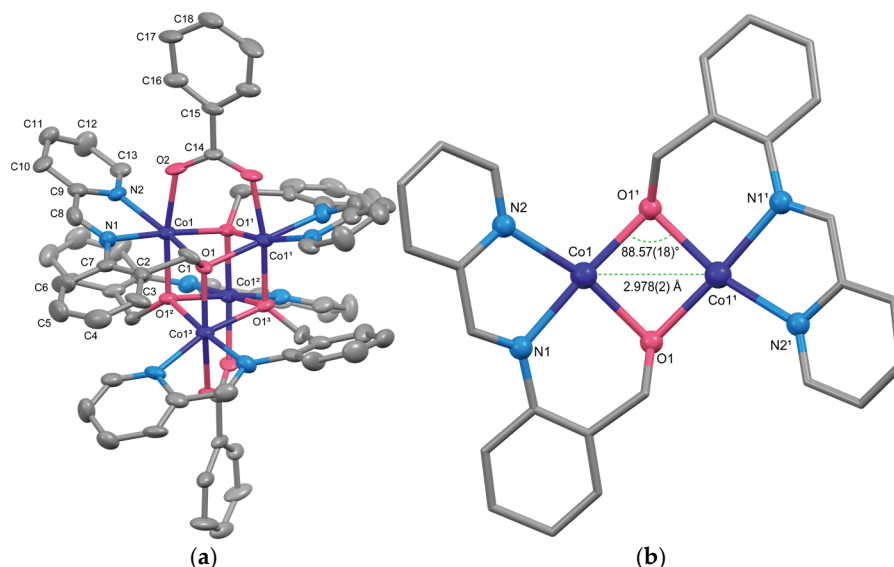


**Figure 4.** (a) Crystal structure for the complex cation of **2**, showing thermal ellipsoids at a 30% probability level. Hydrogen atoms are omitted for clarity. Symmetry code: <sup>(1)</sup>  $1 - x, 2 - y, +z$ ; <sup>(2)</sup>  $3/2 - y, 1/2 + x, 1/2 - z$ ; <sup>(3)</sup>  $-1/2 + y, 3/2 - x, 1/2 - z$ . (b) Structure of the dinuclear unit viewed from the  $\text{Co}_2\text{O}_2$  plane, with the benzoate ligand omitted for clarity.

The intramolecular metal-to-metal distances in **2** are  $\text{Co1}\cdots\text{Co1}^1 = 2.978(2)$  Å and  $\text{Co1}\cdots\text{Co1}^2 = 3.2561(17)$  Å [symmetry code: <sup>(1)</sup>  $1 - x, 2 - y, +z$ ; <sup>(2)</sup>  $3/2 - y, 1/2 + x, 1/2 - z$ ]. The bridging angles around the O1 atom are  $\text{Co1}-\text{O1}-\text{Co1}^1 = 88.57(18)^\circ$ ,  $\text{Co1}-\text{O1}-\text{Co1}^3 = 100.7(2)^\circ$ , and  $\text{Co1}^1-\text{O1}-\text{Co1}^3 = 101.1(2)^\circ$  [symmetry code: <sup>(3)</sup>  $-1/2 + y, 3/2 - x, 1/2 - z$ ]. Compared to **1**, these values suggest that each face of the cubane core in **2** is closer to a square, and that the distortion into a triakis tetrahedron is smaller. Additionally, intra- and intermolecular  $\pi$ - $\pi$  stacking interactions occur between phenyl rings, with a centroid-to-centroid distance of  $3.6284(8)$  and  $3.6729(8)$  Å (Figure 5a). In the crystal packing, the complex cations are arranged in stacks along the  $c$ -axis, forming an ordered 3D structure (Figure S5). This

arrangement creates channels along the *c*-axis, within which the counter anions ( $\text{Cl}^-$ ) are positioned at intervals of 11.424(6) Å (Figure 5b).

**Table 2.** Selected bond distances and angles of **2**.

Bond	Distance/Å	Angle	Angle/°
Co1–O1	2.138(5)	O1–Co1–N2	165.8(2)
Co1–O1 <sup>1</sup>	2.127(5)	O1 <sup>2</sup> –Co1–O2	170.5(2)
Co1–O1 <sup>2</sup>	2.091(5)	O1 <sup>1</sup> –Co1–N1	175.7(2)
Co1–O2	2.077(5)	O1–Co1–N1	88.4(2)
Co1–N1	2.144(7)	N1–Co1–N2	78.6(3)
Co1–N2	2.184(7)	O1–Co1–O1 <sup>2</sup>	87.5(2)
		O1 <sup>2</sup> –Co1–N2	105.6(2)
Co1⋯Co1 <sup>1</sup>	2.978(2)	Co1–O1–Co1 <sup>1</sup>	88.57(18)
Co1⋯Co1 <sup>2</sup>	3.2561(17)	Co1–O1–Co1 <sup>3</sup>	100.7(2)
		Co1 <sup>1</sup> –O1–Co1 <sup>3</sup>	101.1(2)

Symmetry code: (1)  $1 - x, 2 - y, +z$ ; (2)  $3/2 - y, 1/2 + x, 1/2 - z$ ; (3)  $-1/2 + y, 3/2 - x, 1/2 - z$ .

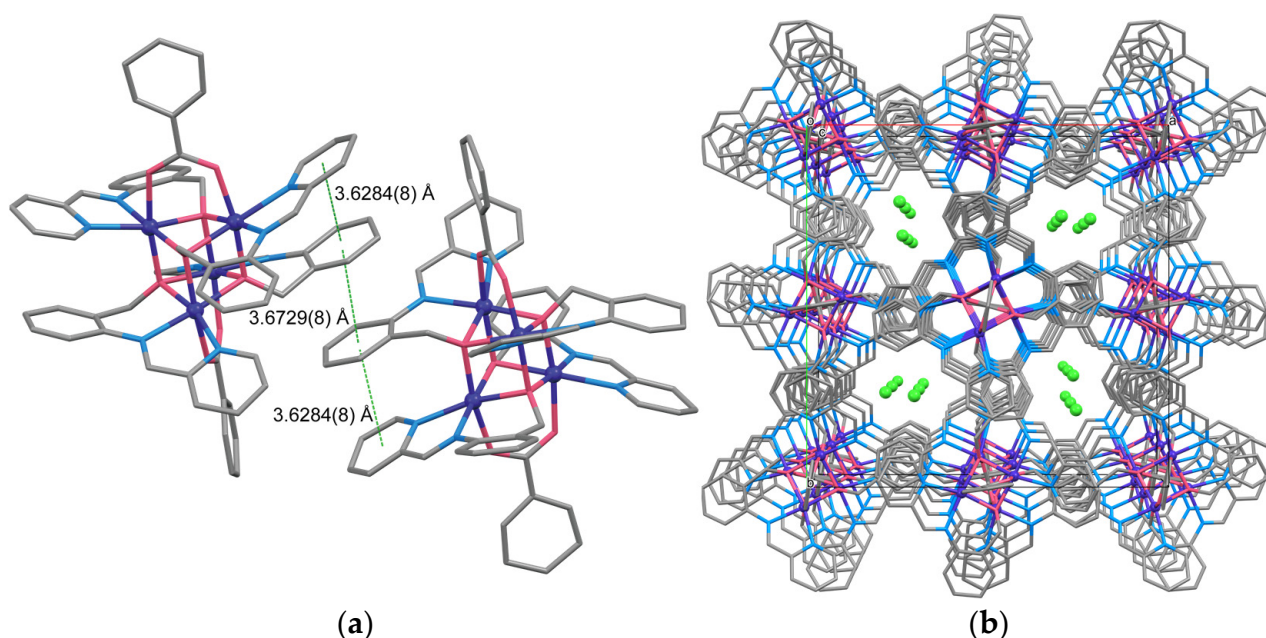


**Figure 5.** (a)  $\pi$ – $\pi$  stacking interactions between two molecular units in **1**. Green dotted lines are guide lines between centroids of aromatic rings. Hydrogen atoms have been omitted for clarity. (b) Packing diagram viewed along the *c*-axis. Chloride anions are shown as light green spheres, and hydrogen atoms have been omitted for clarity.

No clear signals were observed in the powder X-ray diffraction (PXRD) measurements of bulk samples for **1** and **2**, which prevented comparisons with the patterns simulated from single-crystal X-ray diffraction (SCXRD) data. The solvent mask method indicated that both complexes contain crystal solvents within the voids of their 3D structures formed by  $\pi$ – $\pi$  stacking. However, the absence of PXRD signals is likely due to crystal efflorescence caused by the evaporation of these solvent molecules.

### 3.3. Magnetic Properties

Magnetic susceptibility measurements were performed using a SQUID (superconducting quantum interference device) magnetometer. The temperature dependence of the  $\chi_M T$  values for **1** and **2** is presented in Figure 6. At 300 K, the  $\chi_M T$  values for **1** and **2** are 10.73 and 10.56  $\text{cm}^3 \text{mol}^{-1} \text{K}$ , respectively, which are significantly higher than the spin-only value of 7.5  $\text{cm}^3 \text{mol}^{-1} \text{K}$  expected for four uncoupled high-spin Co(II) ions

( $S = 3/2$ ). This increase is attributed to the contribution from orbital angular momentum, resulting from the distorted octahedral geometry of the Co(II) ions. For Complex **1**, the  $\chi_M T$  values remain constant down to 70 K, after which they decrease steadily to  $7.92 \text{ cm}^3 \text{ mol}^{-1} \text{ K}$  at 2 K. This gradual decrease is caused by spin–orbit coupling or zero-field splitting effects. In contrast, the  $\chi_M T$  values of **2** show a steady decline as the temperature decreases, reaching  $0.63 \text{ cm}^3 \text{ mol}^{-1} \text{ K}$  at 2 K. This significant decrease suggests that antiferromagnetic interactions dominate in **2**.

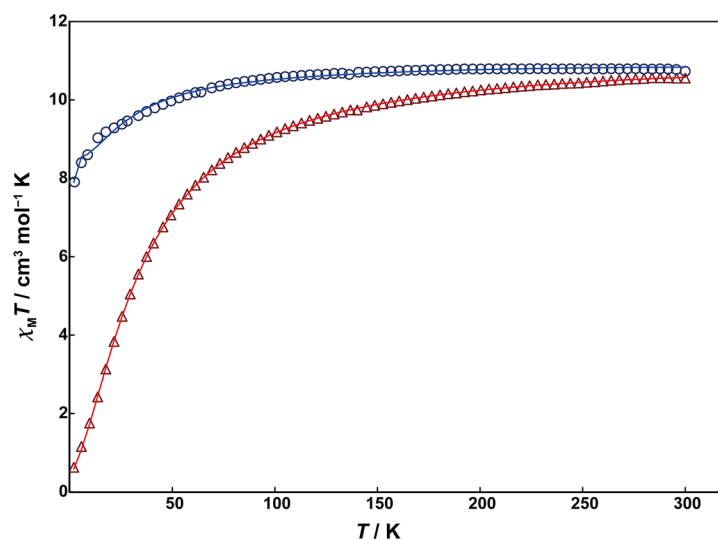


**Figure 6.** Temperature dependence of  $\chi_M T$  vs.  $T$  plots of **1** (blue circles) and **2** (red triangles). Solid lines are drawn with the best-fitted parameter values described in the text.

The interpretation of magnetic exchange interactions in Co(II) complexes is known to be difficult to estimate accurately due to the effects of spin–orbit coupling and zero-field splitting. We initially attempted to fit the data using a simple  $S = 3/2$  tetranuclear cubane model, including the zero-field splitting parameter  $D$  [15]. However, the calculations failed to converge, yielding nonsensical results, as shown in Figure S6. Consequently, we applied the molecular field approximation, treating the cubane structure as a dimer-of-dimers. In this approach,  $J$  represents the interaction within the dinuclear unit, while  $zJ'$  represents the interaction between the dinuclear units. The spin Hamiltonian for the dinuclear unit is expressed in Equation (1), and the corrected susceptibility ( $\chi_{\text{corr}}$ ) obtained through the molecular field approximation is given by Equation (2) [41]. The analysis was performed using the PHI 3.1.6 program [42].

$$H = -JS_1S_2 + \Delta(L_z^2 - 2/3) - (3/2)\kappa\lambda LS + \beta[-(3/2)\kappa L + g_e S]H \quad (1)$$

$$\chi_{\text{corr}} = \frac{\chi}{1 - \left(\frac{zJ'}{N\mu^2}\right)\chi} \quad (2)$$

The obtained magnetic parameters for **1** and **2** are summarized in Table 3, where  $\lambda$  represents the spin–orbit coupling parameter,  $\kappa$  is the orbital reduction factor, and  $\Delta$  is the axial distortion parameter corresponding to the zero-field splitting parameter. In Complex **1**, the magnetic interaction within the  $[\text{Co}_4\text{O}_4]$  core is weak, but the presence of an exceedingly small ferromagnetic interaction is suggested, similar to what has been observed in related complexes [22,28,43,44]. In contrast, Complex **2** is dominated by antiferromagnetic interactions. Typically, simple  $[\text{Co}_4\text{O}_4]$  clusters, such as in **1**, exhibit ferromagnetic interactions due to the orthogonality of the magnetic orbitals, which promotes parallel spin alignment. However, when additional bridging ligands like carboxylate ions are present, as in **2**, antiferromagnetic interactions become predominant due to superexchange pathways facilitated by these ligands [45,46]. Therefore, the differing  $\chi_M T$  behavior of **2** compared to

**1** is attributed to antiferromagnetic interactions caused by the presence of *syn-syn* bridging benzoate ligands.

**Table 3.** Magnetic parameters for **1** and **2**.

Complex	$J/\text{cm}^{-1}$	$J'/\text{cm}^{-1}$	$g$	$\lambda/\text{cm}^{-1}$	$\kappa$	$\Delta/\text{cm}^{-1}$
<b>1</b>	+0.75	−0.015	2.22	−180	0.955	−44.3
<b>2</b>	−6.08	−0.629	2.29	−140	1.09	−6.13

The relatively large negative  $\Delta$  value of **1** is supported by magnetization measurements conducted in the temperature range of 2 to 10 K. The magnetization curve at 2 K does not saturate, even up to 5 T, and the observed value of  $6.7 N\mu_B$  is smaller than the expected value  $12 N\mu_B$  for an  $S = 6$  ground state (Figure 7a). This indicates the presence of strong magnetic anisotropy in the Co(II) ions. The anisotropy is further confirmed by the  $M$  vs.  $H/T$  plot shown in Figure 7b, where the isofield lines do not superimpose, indicating significant magnetic anisotropy in the ground state for **1**. In contrast, the magnetization curve of **2** at 2 K reaches only  $1.7 N\mu_B$ , without saturating even at 5 T (Figure S7a). The curve displays a subtle S-shape, indicative of antiferromagnetic interactions. Due to the small magnetization values, measurements were conducted only at 2 K and 4 K. However, the  $M$  vs.  $H/T$  plots do not overlap on a single curve, suggesting the presence of weak antiferromagnetic interactions or magnetic anisotropy (Figure S7b).

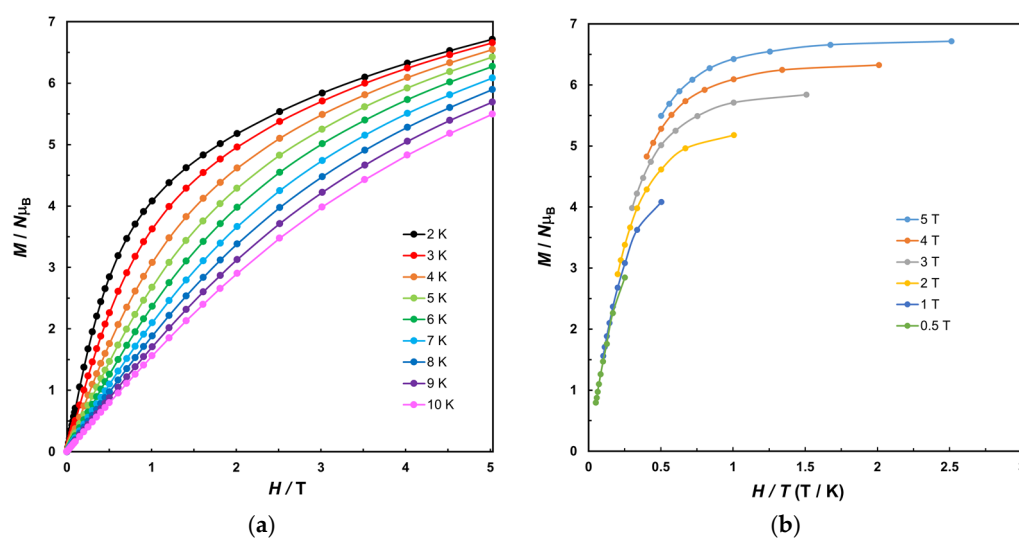


**Figure 7.** Magnetization plots for **1**. (a)  $M$  vs.  $H$  plot in the temperature range of 2 to 10 K; (b)  $M$  vs.  $H/T$  plot in the field range of 0.5 to 5 T. Solid lines are guides for the eye.

Frequency-dependent alternating current (AC) magnetization measurements were performed at frequencies of 1, 10, 100, 500, and 1000 Hz (Figure 8a,b). In the absence of a static DC field, only subtle out-of-phase ( $\chi''_M$ ) signals were detected (Figure S8). However, when an external magnetic field of 2000 Oe was applied, the  $\chi''_M$  component exhibited a significantly larger response and a more pronounced frequency dependence below 5 K, indicating field-induced slow magnetic relaxation. The  $\chi''_M$  responses are similar to those for reported complexes as weak SMMs [22,27,47].

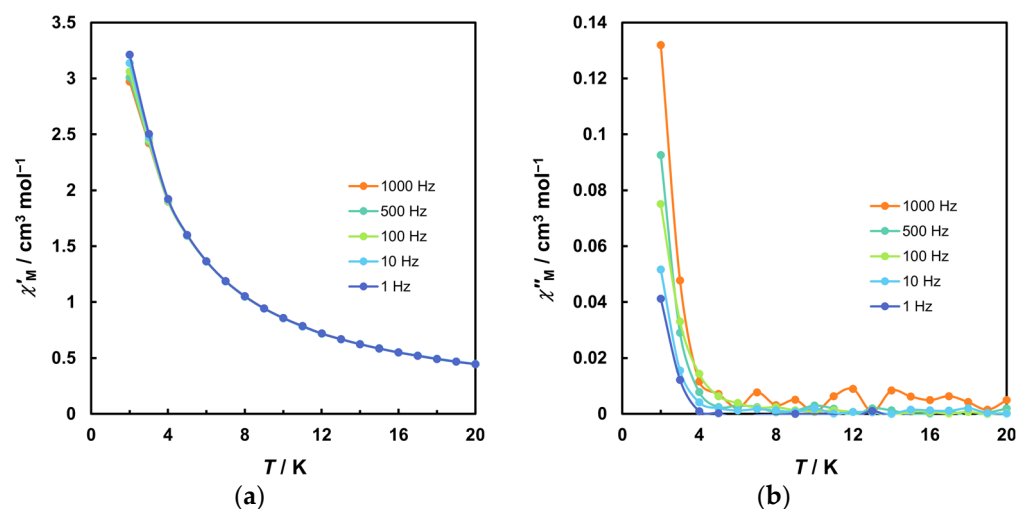


**Figure 8.** Variable temperature AC susceptibility data in a 3 Oe AC field oscillating at 1, 10, 100, 500, and 1000 Hz with 2000 Oe DC static field for **1**. (a) Plot of in-phase ( $\chi'_M$ ) signal. (b) Plot of out-of-phase ( $\chi''_M$ ) signal. Solid lines are guides for the eye.

Since no maximum value was observed in the  $\chi''_M$  graph, a rough estimate of the energy barrier ( $E_a$ ) and pre-exponential factor ( $\tau_0$ ) was attempted using the Debye model via Equation (3) [48–50].

$$\ln \frac{\chi''}{\chi'} = \ln(\omega\tau_0) + \frac{E_a}{k_B T} \quad (3)$$

Figure 9 shows plots of  $\ln(\chi''/\chi')$  versus  $1/T$  for each frequency, based on Equation (3). The resulting lines are not parallel, likely due to correlation errors caused by the ridiculously small  $\chi''$  values or the possibility of multi-relaxation processes. Consequently, it was not possible to estimate the relaxation parameters using this method.

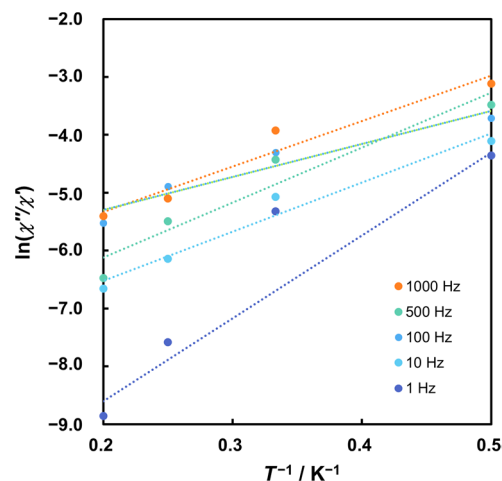


**Figure 9.** Plots of  $\ln(\chi''/\chi')$  versus  $1/T$  for **1** under 2000 Oe DC field. Dotted lines represent linear approximation.

#### 4. Conclusions

New tetranuclear Co(II) complexes **1** and **2**, featuring a  $[\text{Co}_4\text{O}_4]$  cubane core without coordinating solvent molecules, were synthesized via the reaction of  $\text{CoCl}_2 \cdot 6\text{H}_2\text{O}$  with the *NNO* Schiff base ligand Hpmab. The crystal structures of these complexes were elucidated through single-crystal X-ray analysis, revealing that both complexes form tetranuclear cluster based on a dimer-of-dimers structure. The magnetic properties of **1** and **2** were investigated by DC magnetometry, which showed that ferromagnetic interactions dominate in **1**, while antiferromagnetic interactions dominate in **2**. This difference can be attributed

to the presence or *syn-syn* bridging benzoates in **2**, absent in **1**. Additionally, **1** exhibited frequency-dependent out-of-phase signals below 5 K in AC studies, indicating relatively slow magnetic relaxation in magnetization.

**Supplementary Materials:** The following supporting information can be downloaded at: <https://www.mdpi.com/article/10.3390/magnetochemistry10110085/s1>, Table S1. Crystallographic data and refinement parameters. Figure S1. IR spectrum of Hpmb; Figure S2. IR spectrum of **1**; Figure S3. IR spectrum of **2**. Figure S4. Crystal packing diagram of **1**. Hydrogen atoms are omitted for clarity. (a) View along the *a*-axis. (b) View along the *b*-axis. (c) View along the *c*-axis. Figure S5. Crystal packing diagram of **2**. Hydrogen atoms are omitted for clarity. (a) View along the *a*-axis. (b) View along the *b*-axis. (c) View along the *c*-axis. Figure S6. Fitting of the  $\chi T$  curve using an  $S = 3/2$  tetranuclear cubane model. For **1**, the parameters are  $J = 0.989 \text{ cm}^{-1}$ ;  $J' = -0.041 \text{ cm}^{-1}$ ;  $g = 2.45$ ;  $D = -85 \text{ cm}^{-1}$ . For **2**, the parameters are  $J = 1.157 \text{ cm}^{-1}$ ;  $J' = -1.186 \text{ cm}^{-1}$ ;  $g = 2.80$ ;  $D = -488 \text{ cm}^{-1}$ . Figure S7. Magnetization plots of **2**. (a)  $M$  vs.  $H$  plot at 2 and 4 K; (b)  $M$  vs.  $H/T$  plot. Solid lines are guides for the eye. Figure S8. Variable temperature AC susceptibility data in a 3 Oe AC field oscillating at 1, 100, 500, and 1000 Hz under zero applied DC field for **1**. (a) Plot of in-phase ( $\chi'_M$ ) signal. (b) Plot of out-of-phase ( $\chi''_M$ ) signal. Solid lines are guides for the eye.

**Author Contributions:** Conceptualization, M.K.; Data Curation, M.K. and Y.S.; Formal Analysis, Y.S., Y.A., H.Y. and M.O.; Funding Acquisition, M.K.; Investigation, Y.S. and H.Y.; Project Administration, M.K.; Software, M.K.; Supervision, M.K.; Visualization, M.K.; Writing—Original Draft, M.K.; Writing—Review and Editing, M.K. All authors have read and agreed to the published version of the manuscript.

**Funding:** This research received no external funding.

**Institutional Review Board Statement:** Not applicable.

**Informed Consent Statement:** Not applicable.

**Data Availability Statement:** The data that support the findings of this study are available from the author upon reasonable request.

**Acknowledgments:** This research was performed using the equipment (IR and UV-NIR spectroscopy, single-crystal X-ray analysis) of Analytical Research Center for Experimental Science, Saga University. The authors thank the Service Center of the Elementary Analysis of Organic Compounds, Faculty of Science, Kyushu University for elementary analysis.

**Conflicts of Interest:** The authors declare no conflicts of interest. The funders had no role in the design of the study; in the collection, analyses, or interpretation of data; in the writing of the manuscript; or in the decision to publish the results.

## References

1. Sessoli, R.; Gatteschi, D.; Caneschi, A.; Novak, M.A. Magnetic bistability in a metal-ion cluster. *Nature* **1993**, *365*, 141–143. [[CrossRef](#)]
2. McClain, K.R.; Gould, C.A.; Chakarawet, K.; Teat, S.J.; Groshens, T.J.; Long, J.R.; Harvey, B.G. High-temperature magnetic blocking and magneto-structural correlations in a series of dysprosium(III) metallocenium single-molecule magnets. *Chem. Sci.* **2018**, *9*, 8492–8503. [[CrossRef](#)] [[PubMed](#)]
3. Christou, G. Single-molecule magnets: A molecular approach to nanoscale magnetic materials. *Polyhedron* **2005**, *24*, 2065–2075. [[CrossRef](#)]
4. Nayak, S.; Aromí, G.; Teat, S.J.; Ribas-Ariño, J.; Gamez, P.; Reedijk, J. Hydrogen bond assisted co-crystallization of a bimetallic  $\text{Mn}^{\text{III}}_2\text{Ni}^{\text{II}}_2$  cluster and a  $\text{Ni}^{\text{II}}_2$  cluster unit: Synthesis, structure, spectroscopy and magnetism. *Dalton Trans.* **2010**, *39*, 4986–4990. [[CrossRef](#)]
5. Hill, S.; Datta, S.; Liu, J.; Inglis, R.; Milios, C.J.; Feng, P.L.; Henderson, J.J.; del Barco, E.; Brechin, E.K.; Hendrickson, D.N. Magnetic quantum tunneling: Insights from simple molecule-based magnets. *Dalton Trans.* **2010**, *39*, 4693–4707. [[CrossRef](#)]
6. Colacio, E.; Ruiz-Sanchez, J.; White, F.J.; Brechin, E.K. Strategy for the rational design of asymmetric triply bridged dinuclear 3d-4f single-molecule magnets. *Inorg. Chem.* **2011**, *50*, 7268–7273. [[CrossRef](#)]
7. Leuenberger, M.N.; Loss, D. Quantum computing in molecular magnets. *Nature* **2001**, *410*, 789–793. [[CrossRef](#)]
8. Hymas, K.; Soncini, A. Molecular spintronics using single-molecule magnets under irradiation. *Phys. Rev. B* **2019**, *99*, 245405. [[CrossRef](#)]

9. Zabala-Lekuona, A.; Landart-Gereka, A.; Quesada-Moreno, M.M.; Mota, A.J.; Díaz-Ortega, I.F.; Nojiri, H.; Krzystek, J.; Seco, J.M.; Colacio, E. Zero-field SMM behavior triggered by magnetic exchange interactions and a collinear arrangement of local anisotropy axes in a linear  $\text{Co}_3^{\text{II}}$  complex. *Inorg. Chem.* **2023**, *62*, 20030–20041. [[CrossRef](#)]
10. Velkos, G.; Krylov, D.S.; Kirkpatrick, K.; Spree, L.; Dubrovin, V.; Büchner, B.; Avdoshenko, S.M.; Bezmelnitsyn, V.; Davis, S.; Faust, P.; et al. High blocking temperature of magnetization and giant coercivity in the azafullerene  $\text{Tb}_2\text{@C}_{79}\text{N}$  with a single-electron terbium–terbium bond. *Angew. Chem. Int. Ed.* **2019**, *58*, 5891–5896. [[CrossRef](#)]
11. Vieru, V.; Gómez-Coca, S.; Ruiz, E.; Chibotaru, L.F. Increasing the magnetic blocking temperature of single-molecule magnets. *Angew. Chem. Int. Ed.* **2024**, *63*, e202303146. [[CrossRef](#)] [[PubMed](#)]
12. Yang, E.-C.; Harden, N.; Wernsdorfer, W.; Zakharov, L.; Brechin, E.K.; Rheingold, A.L.; Christou, G.; Hendrickson, D.N.  $\text{Mn}_4$  single-molecule magnets with a planar diamond core and  $S = 9$ . *Polyhedron* **2003**, *22*, 1857–1863. [[CrossRef](#)]
13. Gatteschi, D.; Sessoli, R.; Cornia, A. Single-molecule magnets based on iron(III) oxo clusters. *Chem. Commun.* **2000**, 725–732. [[CrossRef](#)]
14. Oshio, H.; Hoshino, N.; Ito, T.; Nakano, M. Single-molecule of ferrous cubes: Structurally controlled magnetic anisotropy. *J. Am. Chem. Soc.* **2004**, *126*, 8805–8812. [[CrossRef](#)] [[PubMed](#)]
15. Yang, E.-C.; Hendrickson, D.N.; Wernsdorfer, W.; Nakano, M.; Zakharov, L.N.; Sommer, R.D.; Rheingold, A.L.; Ledezma-Gairaud, M.; Christou, G. Cobalt single-molecule magnet. *J. Appl. Phys.* **2002**, *91*, 7382–7384. [[CrossRef](#)]
16. Zadrozny, J.M.; Liu, J.; Piro, N.A.; Chang, C.J.; Hill, S.; Long, J.R. Slow magnetic relaxation in a pseudotetrahedral cobalt(II) complex with easy-plane anisotropy. *Chem. Commun.* **2012**, *48*, 3927–3929. [[CrossRef](#)]
17. Vallejo, J.; Castro, I.; Ruiz-García, R.; Cano, J.; Julve, M.; Lloret, F.; De Munno, G.; Wernsdorfer, W.; Pardo, E. Field-induced slow magnetic relaxation in a six-coordinate mononuclear cobalt(II) complex with a positive anisotropy. *J. Am. Chem. Soc.* **2012**, *134*, 15704–15707. [[CrossRef](#)]
18. Guedes, G.P.; Soriano, S.; Comerlato, N.M.; Speziali, N.L.; Lahti, P.M.; Novak, M.A.; Vaz, M.G.F. Two cobalt(II) cubane compounds: The key role of small ligand changes on the crystal packing and magnetic properties. *Eur. J. Inorganica Chem.* **2012**, *2012*, 5642–5648. [[CrossRef](#)]
19. Zhang, S.-H.; Zhang, Y.D.; Zou, H.H.; Guo, J.J.; Li, H.P.; Song, Y.; Liang, H. A family of cubane cobalt and nickel clusters: Syntheses, structures and magnetic properties. *Inorganica Chim. Acta* **2013**, *396*, 119–125. [[CrossRef](#)]
20. Ma, X.-F.; Wang, Z.; Chen, X.-L.; Kurmoo, M.; Zeng, M.-H. Ligand effect on the single-molecule magnetism of tetranuclear  $\text{Co}(\text{II})$  cubane. *Inorg. Chem.* **2017**, *56*, 15178–15186. [[CrossRef](#)]
21. Wu, Y.; Xi, J.; Xiao, T.; Ferrando-Soria, J.; Ouyang, Z.; Wang, Z.; Luo, S.; Liu, X.; Pardo, E. Switching of easy-axis to easy-plane anisotropy in cobalt(II) complexes. *Inorg. Chem. Front.* **2021**, *8*, 5158–5168. [[CrossRef](#)]
22. Modak, R.; Sikdar, Y.; Thuijs, A.E.; Christou, G.; Goswami, S.  $\text{Co}^{\text{II}}_4$ ,  $\text{Co}^{\text{II}}_7$ , and a series of  $\text{Co}^{\text{II}}_2\text{Ln}^{\text{III}}$  ( $\text{Ln}^{\text{III}} = \text{Nd}^{\text{III}}, \text{Sm}^{\text{III}}, \text{Gd}^{\text{III}}, \text{Tb}^{\text{III}}, \text{Dy}^{\text{III}}$ ) coordination clusters: Search for single molecule magnets. *Inorg. Chem.* **2016**, *55*, 10192–10202. [[CrossRef](#)] [[PubMed](#)]
23. Zeng, M.-H.; Yao, M.-X.; Liang, H.; Zhang, W.-X.; Chen, X.-M. A single-molecule-magnetic, cubane-based, triangular  $\text{Co}_{12}$  supercluster. *Angew. Chem. Int. Ed.* **2007**, *46*, 1832–1835. [[CrossRef](#)] [[PubMed](#)]
24. Hill, S.; Edwards, R.S.; Aliaga-Alcalde, N.; Christou, G. Quantum coherence in an exchange-coupled dimer of single-molecule magnets. *Science* **2003**, *302*, 1015–1018. [[CrossRef](#)] [[PubMed](#)]
25. Zhang, S.-H.; Li, N.; Ge, C.-M.; Feng, C.; Ma, L.-F. Structures and magnetism of  $\{\text{Ni}_2\text{Na}_2\}$ ,  $\{\text{Ni}_4\}$  and  $\{\text{Ni}_6^{\text{II}}\text{Ni}^{\text{III}}\}$  2-hydroxy-3-alkoxy-benzaldehyde clusters. *Dalton Trans.* **2011**, *40*, 3000–3007. [[CrossRef](#)]
26. Saseendran, D.P.A.; Fischer, J.W.A.; Müller, L.; Abbott, D.F.; Mougél, V.; Jeschke, G.; Triana, C.A.; Patzke, G.R. Copper(II) defect-cubane water oxidation electrocatalysts: From molecular tetramers to oxidic nanostructures. *Chem. Commun.* **2023**, *59*, 5866–5869. [[CrossRef](#)]
27. Sun, H.; Zhang, J.; Cai, Y.; Liu, W.; Zhang, X.; Dong, Y.; Li, Y. Syntheses, structures, and magnetic properties of a cubane-like  $\{\text{Co}_4\text{O}_4\}$  cluster and a dinuclear  $\text{Cu}^{\text{II}}$  compound constructed from a tridentate Schiff base ligand. *Polyhedron* **2017**, *125*, 135–140. [[CrossRef](#)]
28. Galloway, K.W.; Whyte, A.M.; Wernsdorfer, W.; Sanchez-Benitez, J.; Kamenev, K.V.; Parkin, A.; Peacock, R.D.; Murrie, M. Cobalt(II) citrate cubane single-molecule magnet. *Inorg. Chem.* **2008**, *47*, 7438–7442. [[CrossRef](#)]
29. Koikawa, M.; Ohba, M.; Tokii, T. Syntheses, structures, and magnetic properties of tetranuclear  $\text{Ni}^{\text{II}}_4$  and  $\text{Ni}^{\text{II}}_2\text{Mn}^{\text{III}}_2$  complexes with *ONO* tridentate ligands. *Polyhedron* **2005**, *24*, 2257–2262. [[CrossRef](#)]
30. Fukuda, M.; Eguchi, K.; Matsumoto, K.; Yoneda, K.; Yamada, Y.; Yoshino, H.; Imamura, Y.; Yamamoto, N.; Ohba, M.; Koikawa, M. Novel tetranuclear heterometallic  $\text{Mn}_3\text{Ni}$  and mononuclear  $\text{Ni}$  complexes with an *ONO* Schiff base ligand: Synthesis, crystal structures, and magnetic properties. *Magnetochemistry* **2023**, *9*, 225. [[CrossRef](#)]
31. Selwood, P.W. *Magnetochemistry*; Interscience Publishers: New York, NY, USA, 1956; pp. 78–91.
32. Rigaku Corporation. *CrystalClear: Data Collection and Processing Software*; Rigaku Corporation: Tokyo, Japan, 1998.
33. Rigaku Oxford Diffraction. *CrysAlis Pro*; Rigaku Oxford Diffraction: Tokyo, Japan, 2022.
34. Sheldrick, G.M. SHELXT—Integrated space-group and crystal-structure determination. *Acta Crystallogr. Sect. A Found. Adv.* **2015**, *71*, 3–8. [[CrossRef](#)] [[PubMed](#)]
35. Jiang, J.-S.; Brünger, A.T. Protein hydration observed by X-ray diffraction: Solvation properties of penicillopepsin and neuraminidase crystal structures. *J. Molec. Biol.* **1994**, *243*, 100–115. [[CrossRef](#)] [[PubMed](#)]

36. Sheldrick, G.M. Crystal structure refinement with SHELXL. *Acta Crystallogr. Sect. C Struct. Chem.* **2015**, *71*, 3–8. [[CrossRef](#)] [[PubMed](#)]
37. Dolomanov, O.V.; Bourhis, L.J.; Gildea, R.J.; Howard, J.A.K.; Puschmann, H. OLEX2: A complete structure solution, refinement and analysis program. *J. Appl. Cryst.* **2009**, *42*, 339–341. [[CrossRef](#)]
38. Macrae, C.F.; Sovago, I.; Cottrell, S.J.; Galek, P.T.A.; McCabe, P.; Pidcock, E.; Platings, M.; Shields, G.P.; Stevens, J.S.; Towler, M.; et al. Mercury 4.0: From visualization to analysis, design and prediction. *J. Appl. Crystallogr.* **2020**, *53*, 226–235. [[CrossRef](#)] [[PubMed](#)]
39. Deacon, G.B.; Phillips, R.J. Relationships between the carbon-oxygen stretching frequencies of carboxylato complexes and the type of carboxylate coordination. *Coord. Chem. Rev.* **1980**, *33*, 227–250. [[CrossRef](#)]
40. Llunell, M.; Casanova, D.; Cirera, J.; Alemany, P.; Alvarez, S. *SHAPE, Version 2.1*; University of Barcelona: Barcelona, Spain, 2013.
41. O'Connor, C.J. Magnetochemistry—Advances in theory and experimentation. In *Progress in Inorganic Chemistry*; Lippard, S.J., Ed.; John Wiley & Sons: New York, NY, USA, 1982; Volume 29, pp. 203–283. [[CrossRef](#)]
42. Chilton, N.F.; Anderson, R.P.; Turner, L.D.; Soncini, A.; Murray, K.S. PHI: A powerful new program for the analysis of anisotropic monomeric and exchange-coupled polynuclear *d*- and *f*-block complexes. *J. Comput. Chem.* **2013**, *34*, 1164–1175. [[CrossRef](#)]
43. Murrie, M.; Teat, S.J.; Stöckli-Evans, H.; Güdel, H.U. Synthesis and characterization of a cobalt(II) single-molecule magnet. *Angew. Chem. Int. Ed.* **2003**, *42*, 4653–4656. [[CrossRef](#)]
44. Hudson, T.A.; Berry, K.J.; Moubaraki, B.; Murray, K.S.; Robson, R. Citrate, in collaboration with a guanidinium ion, as a generator of cubane-like complexes with a range of metal cations: Synthesis, structures, and magnetic properties of  $[\text{C}(\text{NH}_2)_3]_8[\text{M}^{\text{II}}]_4(\text{cit})_4 \cdot 8\text{H}_2\text{O}$  (M = Mg, Mn, Fe, Co, Ni, and Zn; cit = citrate). *Inorg. Chem.* **2006**, *45*, 3549–3556. [[CrossRef](#)]
45. Tian, C.B.; Zhang, H.-B.; Peng, Y.; Xie, Y.-E.; Lin, P.; Li, Z.-H.; Du, S.-W. Synthesis, structures, and magnetic properties of three 3D coordination polymers based on  $\text{M}_4\text{O}_4$  cubanes (M =  $\text{Mn}^{\text{II}}$ ,  $\text{Fe}^{\text{II}}$ ,  $\text{Co}^{\text{II}}$ ). *Eur. J. Inorg. Chem.* **2012**, *2012*, 4029–4035. [[CrossRef](#)]
46. Zhang, S.-H.; Ma, L.-F.; Zou, H.-H.; Wang, Y.G.; Liang, H.; Zeng, M.H. Anion induced diversification from heptanuclear to tetranuclear clusters: Syntheses, structures and magnetic properties. *Dalton Trans.* **2011**, *40*, 11402–11409. [[CrossRef](#)] [[PubMed](#)]
47. Bartolomé, J.; Filoti, G.; Kuncser, V.; Schinteie, G.; Mereacre, V.; Anson, C.E.; Powell, A.K.; Prodius, D.; Turta, C. Magnetostructural correlations in the tetranuclear series of  $\{\text{Fe}_3\text{LnO}_2\}$  butterfly core clusters: Magnetic and Mössbauer spectroscopic study. *Phys. Rev. B* **2009**, *80*, 014430. [[CrossRef](#)]
48. Gao, Q.; Qin, Y.; Chen, Y.; Liu, W.; Li, H.; Wu, B.; Li, Y.; Li, W. Cubane-type  $\{\text{M}_4\text{O}_4\}$  (M =  $\text{Co}^{\text{II}}$ ,  $\text{Zn}^{\text{II}}$ ,  $\text{Cu}^{\text{II}}$ ) clusters: Synthesis, crystal structures, and luminescent and magnetic properties. *RSC Adv.* **2015**, *5*, 43195–43201. [[CrossRef](#)]
49. Bhattacharya, P.; Bag, R.; Satpathi, S.; Pati, S.K.; Butcher, R.J.; Tang, J.; Goswami, S. Structure and magnetism of  $\text{Ln}^{\text{III}}_2$  (Ln = Gd, Tb, Dy, and Ho) assemblies constructed from a bis(hydrazone) compartmental ligand: Slow magnetic relaxation in the  $\text{Dy}^{\text{III}}_2$  analogue. *Cryst. Growth Des.* **2023**, *33*, 7459–7471. [[CrossRef](#)]
50. Kalinke, L.H.G.; Rabelo, R.; Valdo, A.K.; Martins, F.T.; Moliner, N.; Ferrando-Soria, J.; Julve, M.; Lloret, F.; Cano, J.; Cangussu, D. Trinuclear cobalt(II) triple helicate with a multidentate bithiazolebis(oxamate) ligand as a supramolecular nanomagnet. *Inorg. Chem.* **2022**, *61*, 5696–5700. [[CrossRef](#)]

**Disclaimer/Publisher's Note:** The statements, opinions and data contained in all publications are solely those of the individual author(s) and contributor(s) and not of MDPI and/or the editor(s). MDPI and/or the editor(s) disclaim responsibility for any injury to people or property resulting from any ideas, methods, instructions or products referred to in the content.